International Journal of Naval Architecture and Ocean Engineering 15 (2023) 100546

Contents lists available at ScienceDirect

International Journal of Naval Architecture and Ocean Engineering

journal homepage: www.journals.elsevier.com/international-journal-of-naval-architecture-and-ocean-engineering/

Dynamic responses and robustness performance to moving boundary of double-stepped cable during deep-sea mining

Yilun Li [a,1], Shuangxi Guo [b,c,1], Yucheng Guo [b,c], Xiaoqi Yu [b,c], Weimin Chen [b,c,*], Jixiang Song [b]

[a] CentraleSupelec, CNRS (UMR9026), LMPS (Paris-Saclay Mechanical Laboratory), Paris-Saclay University, Gif-sur-Yvette, France
[b] Institute of Mechanics, Chinese Academy of Sciences, Beijing, China
[c] School of Engineering Science, University of Chinese Academy of Sciences, Beijing, China

A R T I C L E I N F O

Keywords:
Complex configuration
Double-stepped
Dynamic
Wave propagation
No-uniform structure

A B S T R A C T

As the exploration and exploitation of deep-sea oil and gas, along with promising polymetallic nodule&sulfides mining, have been developing toward ultra-deep waters, some innovative concepts of marine cable configuration suitable for ultra-deepwater are proposed, such as stepped cable, hybrid cable and double-stepped cable. For deep-water cables with complex configurations, the structural responses become more complicated due to their non-uniform structural properties. Because the distributed buoyancy modules along cable length might introduce more significant local bending segments. Moreover, the impacts of moving boundary, caused by the motions of top vessel and bottom mining vehicle, should be considered. Through combing the finite element simulations with the hydrodynamic models, the dynamic response analysis approach of ultra-deepwater cables is established in this study. Then the double-stepped cable responses, including axial tension, displacement along with the change of overall configurations caused by moving top vessel and bottom mining vehicle, are calculated. Moreover, wave propagation behaviors during cable response are comprehensively examined, and the influences of non-uniform structural properties on cable response and wave propagation are analyzed using the wave propagation theory of structure with axially varying properties based on the Bessel function. The results show that the presented double-stepped cable can provide suitable configurations during the dynamic response, which has good compliance performance and can effectively buffer its response caused by moving boundary excitation. Finally, we found that the response spatial-temporal evolutions present some interesting phenomena, such as the axially non-uniform characteristics lead to non-monotonic changes in response amplitude and wavelength, with local peaks occurring in the low-tension region, owing to the distributed buoyancy modules, along with axially-varying and discontinuous structural properties. And, there exists significant mixed effect coming from both standing waves and traveling waves.

1. Introduction

Deep-sea explorations and exploitations, aiming to obtain not only traditional ocean oil and gas, but also some rare deep-sea mineral resources such as manganese metal, other polymetallic nodules and sulfides, have been more and more attractive and significant to the future of energies and human life. These industry operation systems need to serve in the harsh deep-sea environments to complete complex exploration and production tasks, which are usually huge in size and costly expensive systems (Chen et al., 2017; Yu et al., 2022). As one of the important parts of the overall production system, riser and cable transmission systems have been intensely studied, and a variety of deep-water riser/cable configurations have been proposed, including SCR (Steel Catenary Riser), TTR (Top Tension Riser), lazy-wave riser and so on (Moore et al., 2017; Santillan et al., 2010; Ruan et al., 2014). These marine risers and cables could be excited into severe motions due to amid ocean waves, currents along with boundary motions caused by mining vehicles and vessels under operating conditions. On the other hand, due to the increase of structural motion amplitude, its inertia force and fluid dynamics become more apparent, which leads to the motion

Peer review under responsibility of The Society of Naval Architects of Korea.
* Corresponding author. Institute of Mechanics, Chinese Academy of Sciences, Beijing, China.
E-mail address: wmchen@imech.ac.cn (W. Chen).
[1] These authors equally contributed to this work.

https://doi.org/10.1016/j.ijnaoe.2023.100546
Received 14 April 2023; Received in revised form 24 June 2023; Accepted 3 August 2023
Available online 12 August 2023

response and the variation of tension and stress becoming more complex. In order to have better operation and service life of these risers, it is crucial to comprehensively and carefully examine cable configurations and to analyze dynamic structural performances under excitation of boundary motions, and also, this work can provide the basis for detailed structural design and analysis.

Now, there are abundant research on dynamic response analysis and structural design of flexible marine structures (Lee et al., 2015; Adamiec-Wojcik et al., 2015; Vásquez and Avila, 2021; Leonardo et al., 2022; Lou et al., 2019; Fu et al., 2019; Wang and Duan, 2015; Tang et al., 2015). Based on the principles of virtual work and variation, Lou (Lou et al., 2019) studied the tension and stress distribution characteristics of static compliant cables and analyzed the influence of buoyancy distribution on cable configuration. Wang (Wang and Duan, 2015) investigated the impacts of ocean current and internal flow on steel lazy-wave riser's static performance with the finite difference method. With the increase of water depth and cable length, their dynamic characteristics become more pronounced, and researchers began to use dynamic methods to design and study the structural response under environmental loads. Yin (Yin et al., 2018) studied the dynamic responses of a TTR with vessel motion using both model tests and numerical simulation, and he pointed out that the dynamic responses consists of both in-line responses and cross-flow vortex-induced vibrations. Cheng (Cheng et al., 2020) proposed a time-domain numerical method to study the dynamic characteristics of steel lazy wave risers under vessel motion and wave-current loads, and he studied the influence of buoyancy distribution length on the riser's dynamic characteristics. Mansour (Mansour et al., 2018) obtained the exact expression of catenary cable curvature by considering first-order geometric nonlinearities, and he found that new dynamic features, such as additional hybrid modes and internal resonances, may emerge. Hsu (Hsu et al., 2017) studied the dynamic tension of a mooring system caused by floating offshore wind turbine motion, and the results showed that typical snap event was found because of a temporary slackness in the line, and the maximum tension values recorded are 37%–68% higher than the corresponding cyclic non-snap tension. Cabrera (Cabrera and Paik, 2019) studies the nonlinear planar vibrations of a steel lazy wave riser excited by slug flow using the Euler-Bernoulli beam model and steady plug-flow model. Using a linear stability analysis, Kim (Kim and O'Reilly, 2019) showed how the internal fluid can destabilize specific static configurations of a catenary-type flexible riser. Oh (Oh et al., 2020) analyzed the effective parameters on the responses of steel lazy wave risers using multibody dynamic simulation, and he developed a simulation-based design framework for shape design.

As the exploration and exploitation of deep-sea oil and gas, along with promising polymetallic nodule&sulfides mining, have been developing toward ultra-deep waters, some innovative concepts of marine cable configuration suitable for ultra-deepwater are proposed, such as stepped cable, hybrid cable and double-stepped cable (Kim and O'Reilly, 2019; Tian et al., 2015; Chen et al., 2021). However, fewer reports on comprehensive dynamic characteristics analysis, particularly its wave propagation behaviors of ultra-deep-water cables with axially varying properties, are seen. Some of the current studies mainly focus on structural design and static configuration analysis (Lou et al., 2019; Chen et al., 2021). As we know, for cables with complex configurations, their dynamic response becomes more complicated due to the discontinuity and axially varying properties of the cable structure, along with the considerable bending and overhanging section in some local areas. Moreover, moving boundary impacts caused by the motions of top-vessel and bottom-mining vehicles are significant. Therefore, it is necessary to comprehensively evaluate the response of double-stepped configuration cable under environmental excitation and analyze the spatial-temporal evolution characteristics and mechanism of the riser's responses. Through combing the finite element simulations with the hydrodynamic models, the dynamic response analysis approach of ultra-deepwater cables is established in this study. Then the double-stepped cable responses, including axial tension, displacement along with change of overall configurations caused by moving top vessel and bottom mining vehicle, are calculated. Moreover, wave propagation behaviors during cable response are comprehensively examined, and the influences of non-uniform structural properties on cable response and wave propagation are analyzed using the wave propagation theory of structure with axially-varying properties.

2. Model descriptions of flexible cable with distributed buoyancy modules

2.1. Finite element structural model combined with the hydrodynamic model

The double-stepped configuration (Fig. 1) is proposed for ultra-deepwater cables in the oil, gas and mining industries. Through carefully designing distributions of the buoyancy modules along the cable's length, the overall configuration has several sag bend and hog bend zones. Thus, the double-stepped cable has better response behaviors when it suffers excitations coming from environmental loads and top/bottom-end (top vessel and bottom mining vehicle) motions. Therefore, the optimizations of modules' position and buoyancy value become more complicated, and comprehensive and accurate calculations of the dynamic response of double-stepped cable during mining operations are pretty important.

Different from previous uniform cables, because several floating modules are distributed along the cable length, cable configuration becomes more complex. And, the fluid-structure interaction becomes more complicated (Tian et al., 2015; Chen et al., 2021; Guo et al., 2022). Moreover, besides fluid load coming from amid sea current, due to the movement of the bottom mining vehicle and top vessel, the cable may experience a relative motion to the surrounding fluid. Thus, its hydrodynamic force should be particularly considered. Here, we employed the hydrodynamic model to express the coupling force, which is based on the characteristics of structural reconfiguration and dragging reduction of this non-uniform cable (Gosselin et al., 2010; Vogel, 2015; Leclercq et al., 2018; Jacobsen et al., 2019; Leclercq and De Langre, 2018). The existing researches, considering the effect of structural reconfiguration and fluid drag reduction, mainly focus on uniform structures, such as cantilever beam and plate, or continuous deformation structures such as trapezoidal beam. Regarding non-uniform cable, Song (Song et al.,

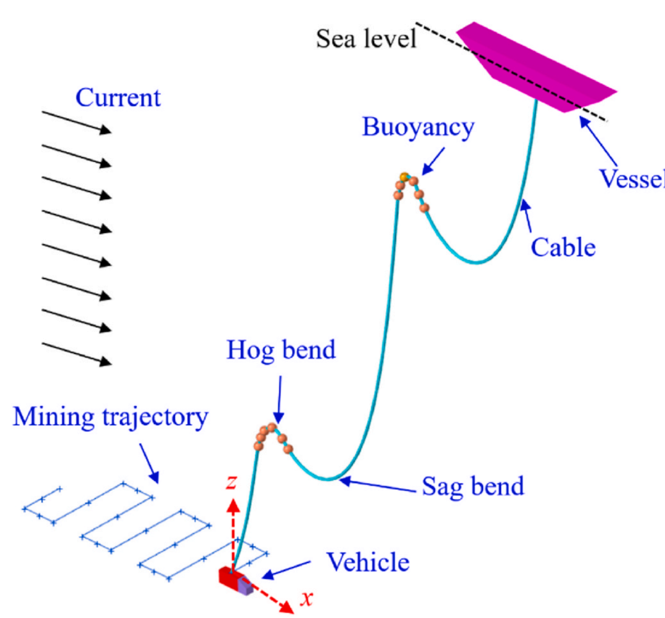

Fig. 1. Schematic of double-stepped cable.

2021) and Guo (Chen et al., 2021) respectively studied the cantilever beam containing a buoyant sphere, and they obtained a reasonable hydrodynamic model. Here, we will extend this method to the cable with distributed buoyancy modules. And we will verify the approach by comparing it with the experimental results of ours and other's. Our hydrodynamic coupling model and the FEM structural model will be introduced briefly.

The governing equation of a cable with floating spherical modules is (Guo et al., 2022)

$$\frac{\partial^3\theta}{\partial s^3}=\frac{1}{EI}\left\{\left[mg-f_{\text{buoyancy}}-f_{\text{buoyBall}}\delta(s-s^*)\right]\sin\theta+\frac{1}{2}C_D\rho(U\cos\theta)^2D\right\} \quad (1)$$

where θ is the deformation angle of the cable, and s is the cable length. EI *is* the bending stiffness, and mg is the cable weight per unit length. And, $f_{buoyancy}$ is the uniform buoyancy acting the cable, $f_{buoyball}$ is the buoyancy of the modules ball, and $s*$ is the location of buoyancy modules. ρ is the fluid density, D is the cable diameter, U is the fluid velocity, and C_D is the drag coefficient.

The governing Eq. (1) can be written in terms of a non-dimensional form as follow

$$\frac{\partial^3\theta}{\partial s^3}=-B\sin\theta-B_b\delta(1-s')\sin\theta+C_Y\cos^2\theta \quad (2)$$

where $B=\dfrac{L^3(mg-f_{\text{buoyancy}})}{EI}$ $f_{\text{buoyancy}}=\dfrac{1}{4}\rho\pi D^2g$ $s'=\dfrac{s}{L}$ $C_Y=\dfrac{C_D\rho U^2DL^3}{2EI}$ and L is the total length of the structure. The Cauchy number C_Y means the ratio of hydrodynamic drag force to the restoring force owing to structural stiffness. Then, the cable deformation and its reconfiguration under fluid force can be obtained by numerically solving Eq. (2). And the total dragging force exerted on the structure can be calculated by integrating the fluid force in the flow direction along the cable length (Guo et al., 2022)

$$F=\int_0^L\frac{1}{2}C_D\rho(U\cos\theta)^2D\cos\theta\,ds \quad (3)$$

Further, the reconfiguration number R is used, which is defined as the ratio of the drag force of a flexible structure to that of the rigid structure with the same geometric shape. This reconfiguration number R is used to essentially represent the influence of flexibility on drag force $R=F/\left(\frac{1}{2}\rho C_DLDU^2\right)$. Then we can obtain $R=\int_0^1\cos^3\theta ds$. The fluid force acting on flexible cable can be obtained by solving Eq. (1), Eq. (2) and Eq. (3). And it can be expressed as $F\propto U^{2+\upsilon}$, where the Vogel exponents (Oh et al., 2020) can be obtained by the formula of $\upsilon=2\frac{\partial\log R}{\partial\log C_Y}$. After we get the Vogel exponents, we can calculate the fluid-structure coupling force acting on the cable involving structure reconfiguration and fluid drag reduction.

In our FEM structural model, the whole riser is divided into a set of specially defined beam elements (Chen et al., 2021), which is developed to simulate the large displacements of this non-uniform flexible cable, and the fluid-structure coupling force, as mentioned above, can be conveniently loaded on these beam elements. Considering the structural discontinuity caused by floating bodies distributing along the cable

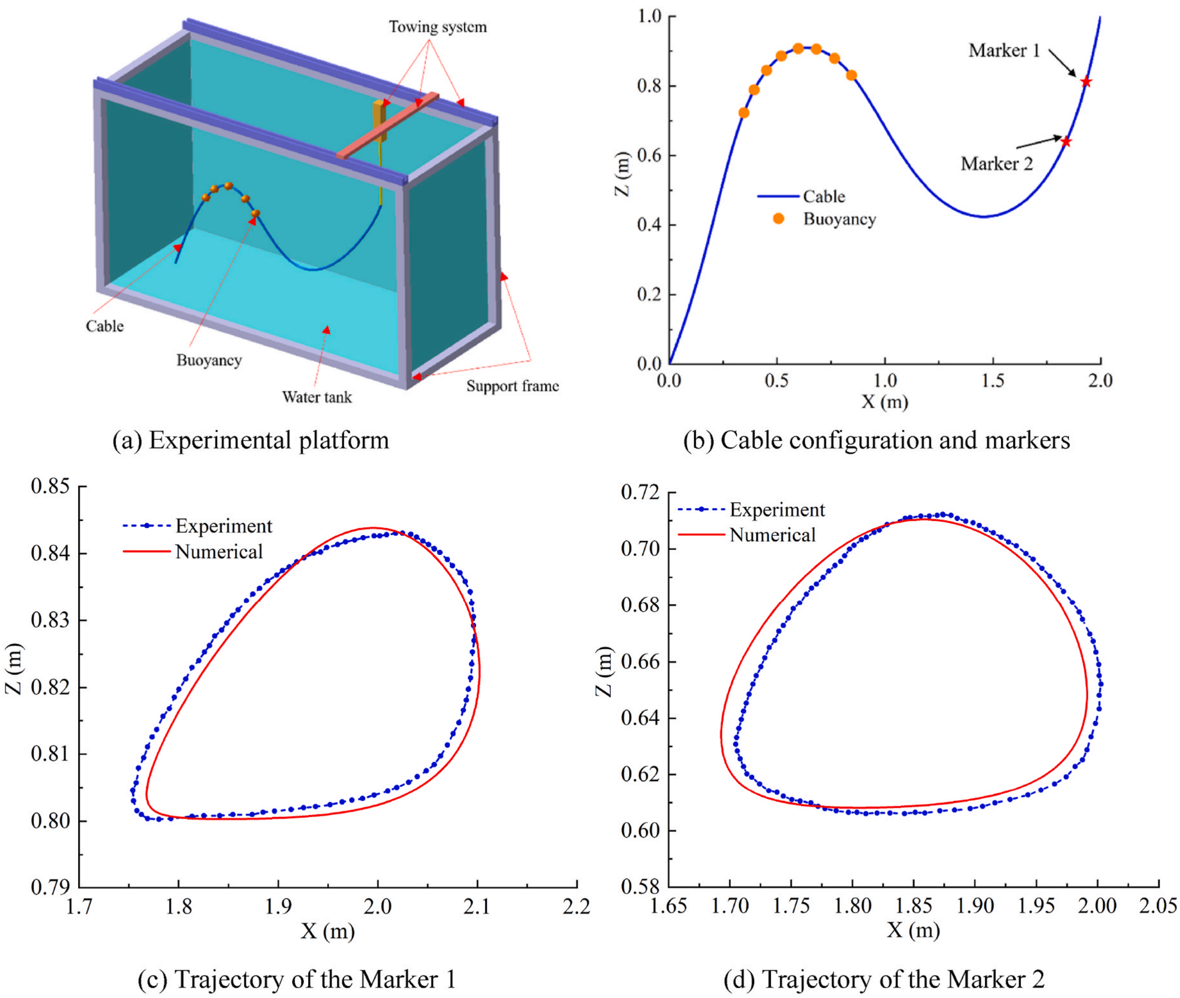

Fig. 2. Comparisons of cable trajectories between numerical and experimental results.

length, the FEM model of this cable is improved by changing the corresponding element values of those nodes with buoyancy, and including the changes of structural mass, stiffness and load parameters during dynamic response analysis. For example, the mass matrix of the conventional beam element is calculated using Eq. (4).

$$
\begin{aligned}
K_e^1 &= \int_0^{l_e}\int_{A_e} B_1^T E B_1 dA_e dx_e \quad M_e^1 = \int_0^{l_e}\int_{A_e} B_1^T \rho A_e B_1 dA_e dx_e \\
K_e^2 &= \int_0^{l_e}\int_{A_e} B_2^T E B_2 dA_e dx_e \quad M_e^2 = \int_0^{l_e}\int_{A_e} B_2^T \rho A_e B_2 dA_e dx_e
\end{aligned}
\tag{4}
$$

where A_e is the cross area, B is the strain matrix, ρ and E are the density and modules of the cable, and l_e and x_e are element length and the axial location. As for the beam elements connected with buoyancy modules, the mass of buoyancy modules should be added to the corresponding mass matrix

$$
\begin{aligned}
M_e^1 &= \int_0^{l_e}\int_{A_e} B_1^T \rho A_e B_1 dA_e dx_e + M_0 \cdot diag\left[\delta_i \quad \delta_{i+1}\right] \\
M_e^2 &= \int_0^{l_e}\int_{A_e} B_2^T \rho A_e B_2 dA_e dx_e + M_0 \cdot diag[\delta_i \quad \delta_i \quad 0 \quad 0 \quad \delta_{i+1} \quad \delta_{i+1} \quad 0 \quad 0]
\end{aligned}
\tag{5}
$$

where M_0 is the mass of each buoyancy module, δ_i is a Dirac function, and its value is 1 if the node contains a buoyancy module, or 0 otherwise. Lastly, by assembling the element matrices, we can obtain the dynamic governing equation of the flexible cable.

2.2. Verifications of the FEM model

To verify the developed model, here, the dynamic responses of two cable configurations, i.e., a stepped cable (Fig. 2(a)) and a catenary cable (Fig. 3(a)), are compared with the experiments. Firstly, the dynamic response of a stepped cable with distributed buoyancy under top-end excitation is experimentally tested and compared with our FEM model. Fig. 2(a) shows the experimental setup, and the cable parameters are listed in Table 1. During experiments, the top-end surge (X direction) period is 3.16s and amplitude is 0.2 m, the trajectories of two markers (see Fig. 2)b), respectively located at 0.2 m (Marker 1) and 0.4 m (Marker 2) measuring from the top-end, are recorded during the experiment. The comparison of the trajectories at two markers are shown in Fig. 2(c) and (d) respectively. The numerical results is displacements of one cycle, and the experimental results are the average values of multiple cycles. It can be seen that the displacement responses agree well with the experimental results.

To further verify the calculated results, in addition to displacement response, the top tension response of a catenary cable is calculated and compared with the experimental results. The cable parameters are provided in Table 2 (JoséAzconaXabier et al., 2017), and Fig. 3(a) shows a schematic diagram of the structure. In the experiment, the surge displacement of the top-end is 0.125 m, and the period is 1.58s. The position at the marker, i.e., located at 2.646 m from the top-end, is compared in Fig. 3(b), and the comparison of top tension is presented in Fig. 3(c). It can be seen that both the displacement responses and tension agree well with the experimental results. And other verifications can be found in the authors' published study (Li et al., 2020).

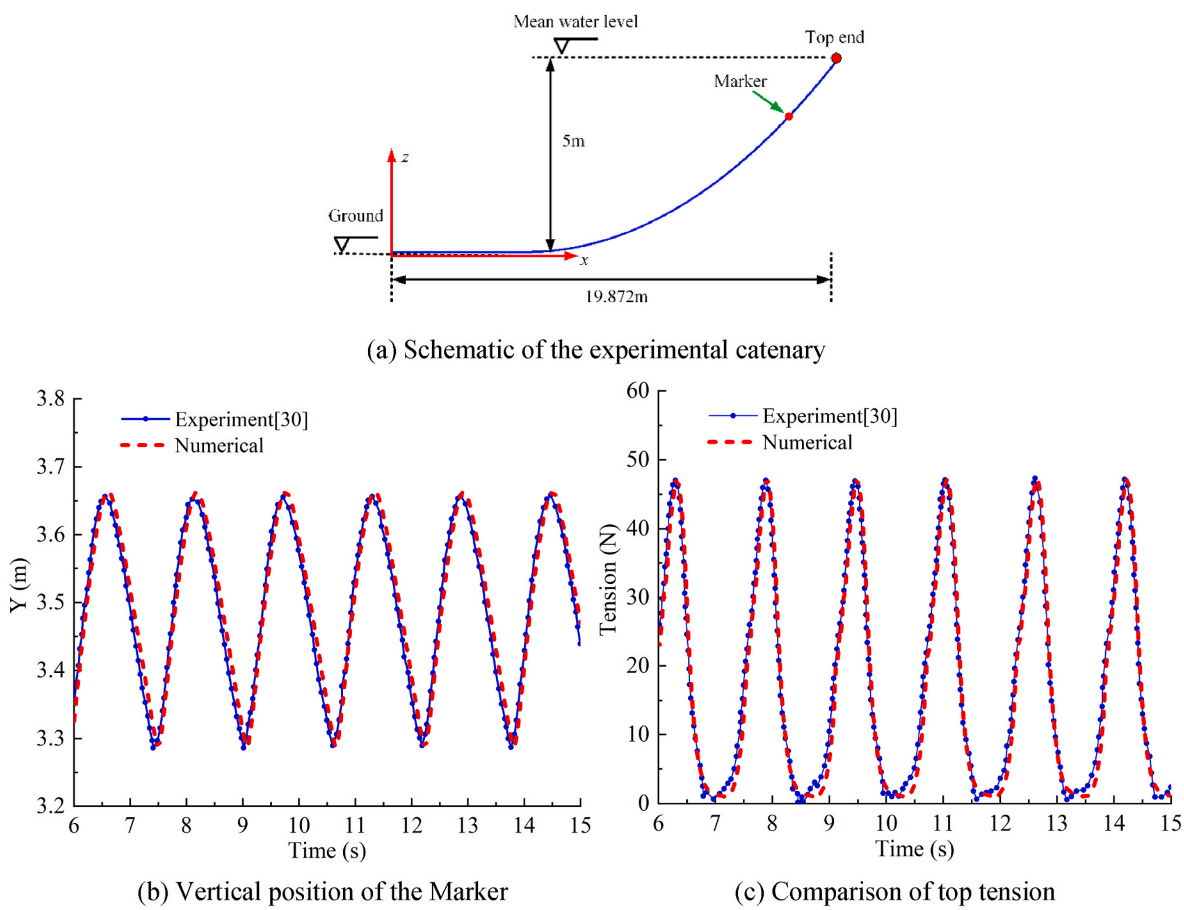

Fig. 3. Comparison of displacement and tension response between numerical and experimental results.

Table 1
Parameters of the stepped cable.

Parameter	Value	Parameter	Value
Total length	3.0 m	Mass per unit length	0.27 kg/m
Initial horizontal projection	2.0 m	Wet weight per unit length	0.22 kg/m
Initial vertical projection	1.0 m	Total buoyancy	5.17 N
Axial stiffness	2.246e5N	Location of buoyancy	0.8–1.4 m
Equivalent hydrodynamic diameter	0.004 m		

Table 2
Parameters of the catenary cable.

Parameter	Value
Total length	21.0 m
Initial vertical projection	5.0 m
Axial stiffness	3.4e5N
Equivalent hydrodynamic diameter	3.4 mm
Mass per unit length	0.069 kg/m
Wet weight per unit length	0.5872 N/m

3. Dynamic responses of the cable under conditions of moving boundaries

Based on our FEM simulations, the cable responses caused by the movement of the top vessel and the bottom mining vehicle are calculated, and the evolutions of structural tension, displacement and configuration are examined. The diagram of the cable and locations of six key points, i.e., points p1-p6, are shown in Fig. 4, and the main structural/material parameters are provided in Table 3. The cable is a

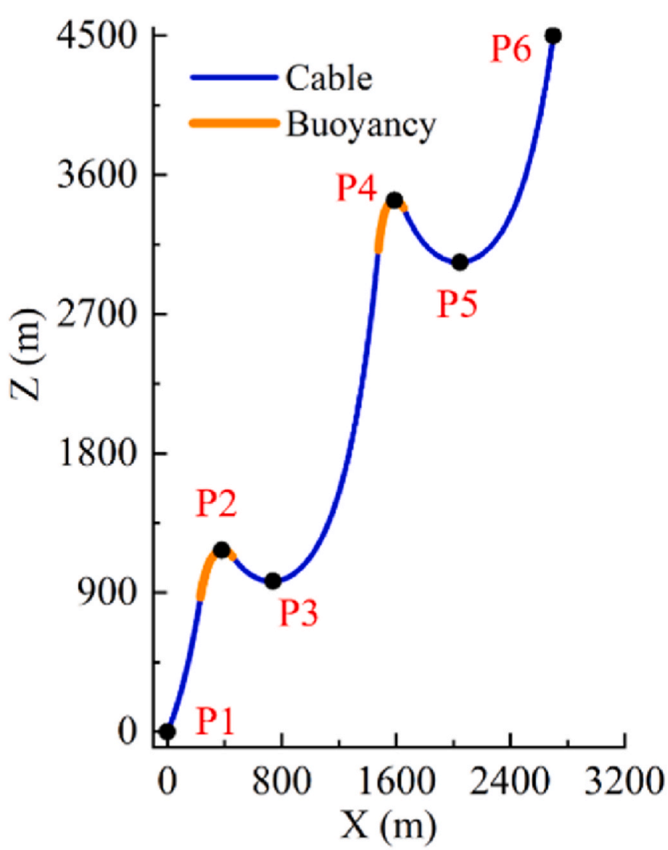

Fig. 4. Configuration and key points of the deep-water cable, where point p1-p6 indicate the six key point of which the displacement and tension are examined.

Table 3
Structural parameters of double-stepped cable.

Parameter	Value	Parameter	Value
Outer diameter	33.6 mm	Underwater weight	2.4 kg/m
Bending stiffness	82.0 N*m2	Safe load limit	125 kN
Axial stiffness	39.3e3 kN	Minimum bending radius	0.95 m
Total length	6750 m	Water depth	4500 m
Horizontal projection	2700 m		

composite structure of which the inner part is made of several metal lines and filling materials, and the outer part is wrapped by a polymer layer.

3.1. *Cable response excited by mining operations*

The cable responses caused by the movement of the mining vehicle are calculated, while it is assumed that the vehicle moves in the XY plane (see Fig. 1) during mining operations. The trajectory of the mining vehicle, running at a speed of 0.2 m/s, is shown in Fig. 5(a). Fig. 5)b presents the plot of the bottom tension of the cable, and it is seen that the tension values oscillate with larger amplitude, i.e., 8 kN, in short-term during the movement of the vehicle. The maximum cable tension is about 24 kN under mining vehicle motion, and it is much smaller than the 125 kN safe load limit (in Table 3) of the cable. If comparing the time history of vehicle position (in Fig. 4(a)) and that of cable tension (in Fig. 5(b)), it can be seen that the short-time oscillation of tension almost occurs as the running direction of the mining vehicle changes. The reason for this tension oscillation may be that the steering turn-around of the mining vehicle causes a short-time larger acceleration, in the original direction of cable motion. This large acceleration might consequently result in an increase of cable tension. Therefore, it would be worthwhile to point out that, in practical mining operations, the actual route of the mining vehicle and the bottom tension of the cable should be accurately designed and evaluated to prevent the bottom tension oscillation with a larger amplitude. Particularly, if bottom tension gets larger than the vehicle weight, it may result in the vehicle being lifted and introduce dangerous structural damage.

Fig. 6 shows the motion trajectories, in the XY plane, of the four points among the buoyancy distribution area. It can be seen that the displacement amplitude of the four points gradually decreases as their position gets far away from the bottom end. Compared with the maximum displacement of 400 m in the X direction of Point 2, the maximum displacement of Point 5 in the X direction is only about 125 m. In addition, it can be seen that when the motion direction of the node changes from Y to X direction, there will still be oscillation displacement in the Y direction, resulting in the short-term oscillation of tension with a relatively large amplitude. This oscillation can also be seen from the node tension presented in Fig. 7, similar to the bottom end, the tension of Point 2 has a short-term oscillation with large amplitude during the first steering of the mining vehicle, and the tension fluctuation decreased significantly in the subsequent response process.

Due to the compliance of the Double-Stepped cable, the dynamic effect of bottom excitation attenuates gradually in the process of upward propagation, so the tension of Points 3 and 4 does not have a large amplitude. Moreover, from Fig. 7(b) it can be seen that the node tension increases gradually with the increase of the X-direction displacement of the vehicle, and the vehicle's Y-direction movement hardly changes the cable tension. The results show that the presented double-stepped cable can provide suitable configurations during the dynamic response, which has good compliance performance and can effectively buffer its response caused by moving boundary excitation.

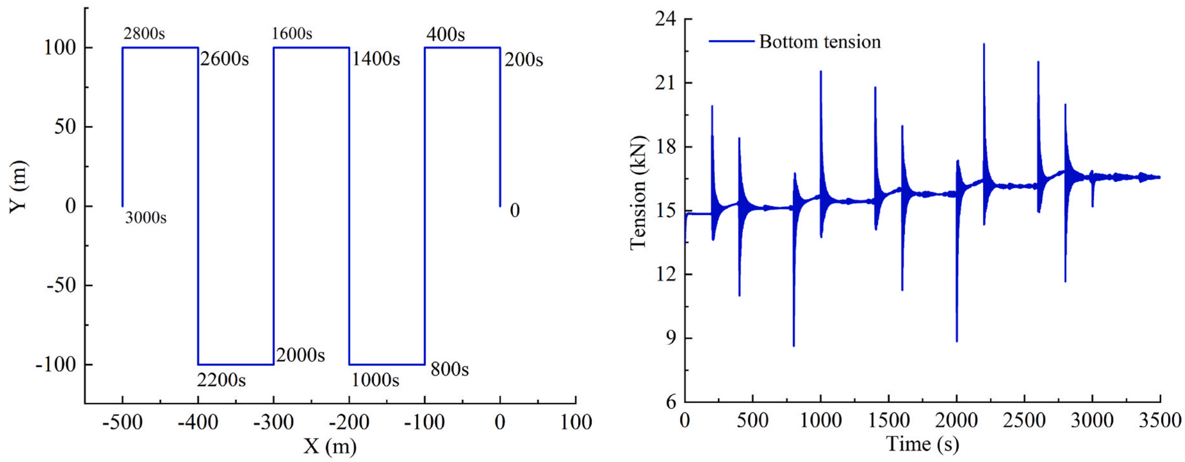

(a) Trajectory of mining vehicle (b) Time history of bottom tension

Fig. 5. Trajectory of mining vehicle and bottom tension.

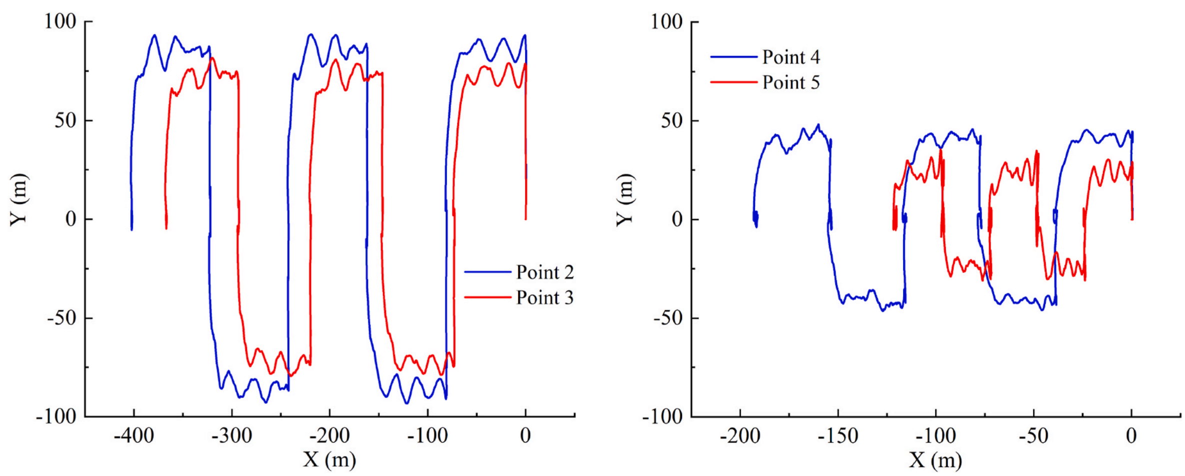

Fig. 6. Trajectories (in XY plane) of four key points along cable length.

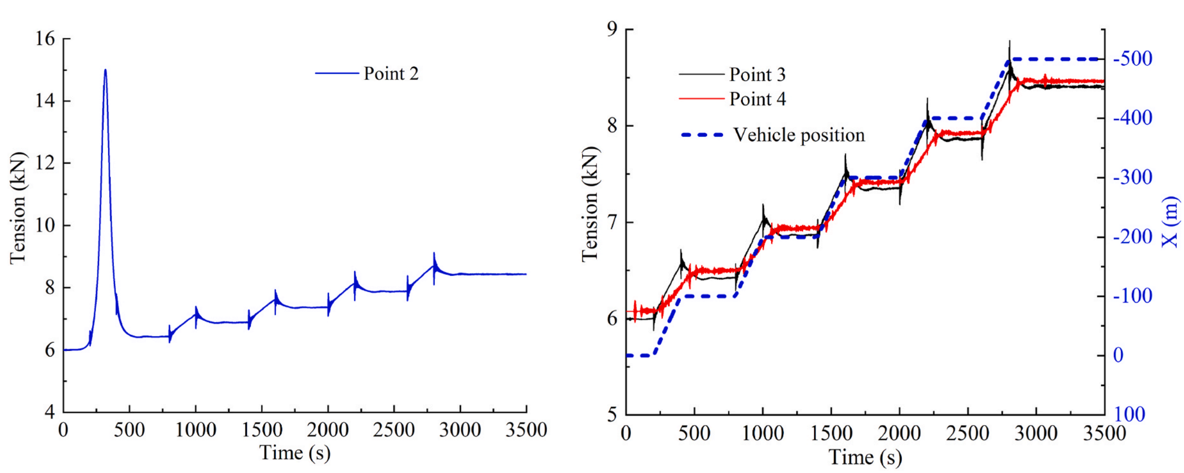

(a) Time history of Point 2 (b) Tension variation of Points 3 and 4

Fig. 7. Structural tension of typical key points.

3.2. Cable response under moving top-vessel

In the actual operation condition, in addition to the boundary excitation caused by the mining vehicle, the movement of the top vessel will also cause a dynamic response of the cable. During the analysis of cable responses caused by top-end vessel motion, two cases are considered. In Case 1, the vessel moves with long period and large value (500s period and 500 m amplitude). In Case 2, the vessel moves periodically under the frequency of regular waves.

3.2.1. Cable response under large vessel amplitude

The cable response is calculated under the motion excitation of the top end vessel with a 500s period and 500 m amplitude in the X direction. Fig. 8(a) shows the tension distribution of the cable in the initial state. The maximum static tension is about 56 kN, which is much smaller than the breaking load of material. The tension in hog bend and sag bend zones is relatively small, because the buoyancy of the buoyancy modules balances the cable's gravity. The positions and configurations of the cable at different times are shown in Fig. 8(b), under the current excitation condition, the cable is in a stable periodic motion state. The cable displacement in the range between Point 4 and Point 6 is apparent, and the response decreases gradually in the process of downward propagation. So we may say that the double-stepped configuration has better compliance performance and can effectively buffer its response caused by moving boundary excitation.

Fig. 9 shows the tension time histories of key points, it can be seen that the point closer to the bottom has a smaller variation range of tension, because the top excitation gradually attenuates in the process of propagating to the bottom end. This response attenuation can also be seen from the motion trajectories of several key points shown in Fig. 10. From the top to the end (point 5 to Point 2), the motion amplitude gradually decreases, and the motion amplitude of Point 2 is only about 10% of the top excitation amplitude. In addition, it can be seen from Fig. 8(a) that the tension time history of Point 2 and Point 3 is basically the same, indicating that the cable response near this position is quasi-static. The results of tension and trajectory further show that the double-stepped configuration cable has good compliance to boundary excitation.

Different from tension responses of other points, the time history of top tension has prominent high-frequency components under the condition of vessel motion (Fig. 11(a)). The tension amplitude of double frequency term is higher than that of excitation frequency (Fig. 11(b)). Because the cable is affected by fluid damping during motion, which is proportional to the square of the cable's velocity, i.e., proportional to

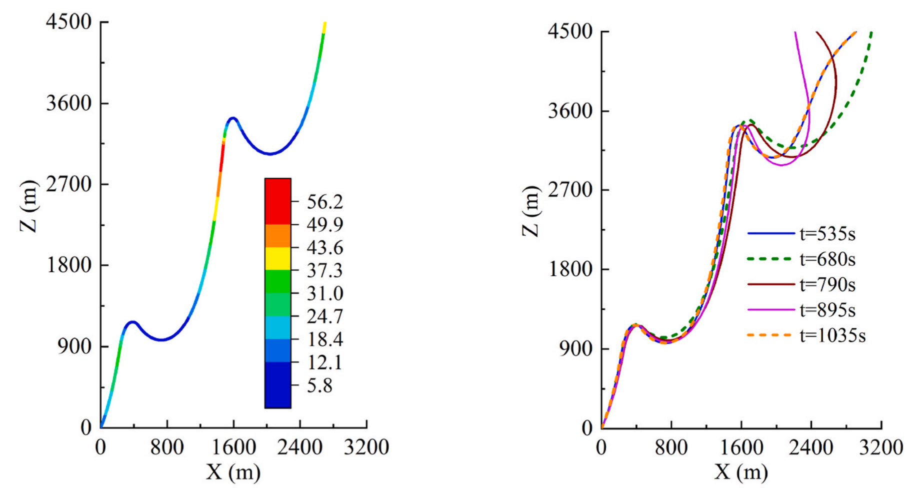

(a) Tension distribution (b) Variation of cable configurations

Fig. 8. Tension distribution and position variation of the cable.

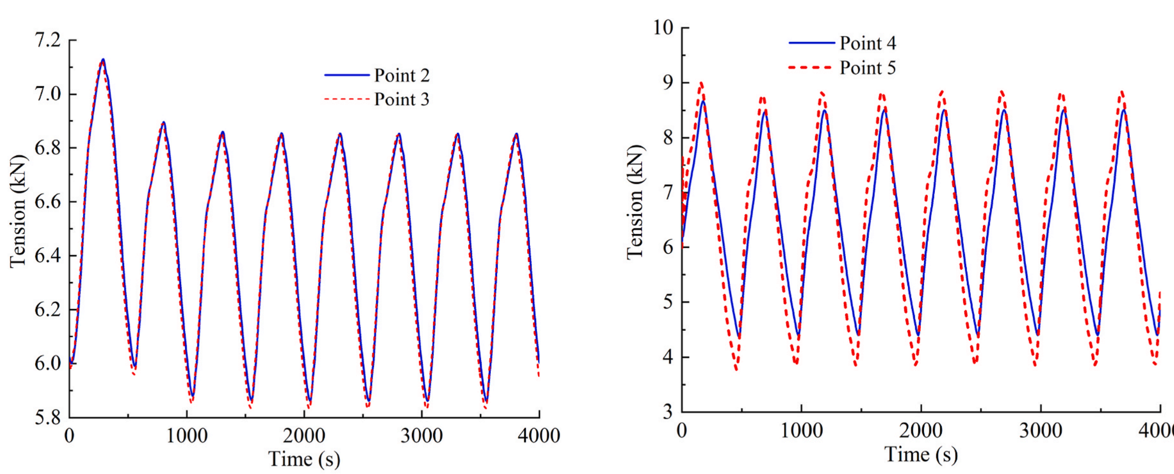

(a) Tension history of point 2 and 3 (b) Tension history of point 4 and 5

Fig. 9. Tension history of key points.

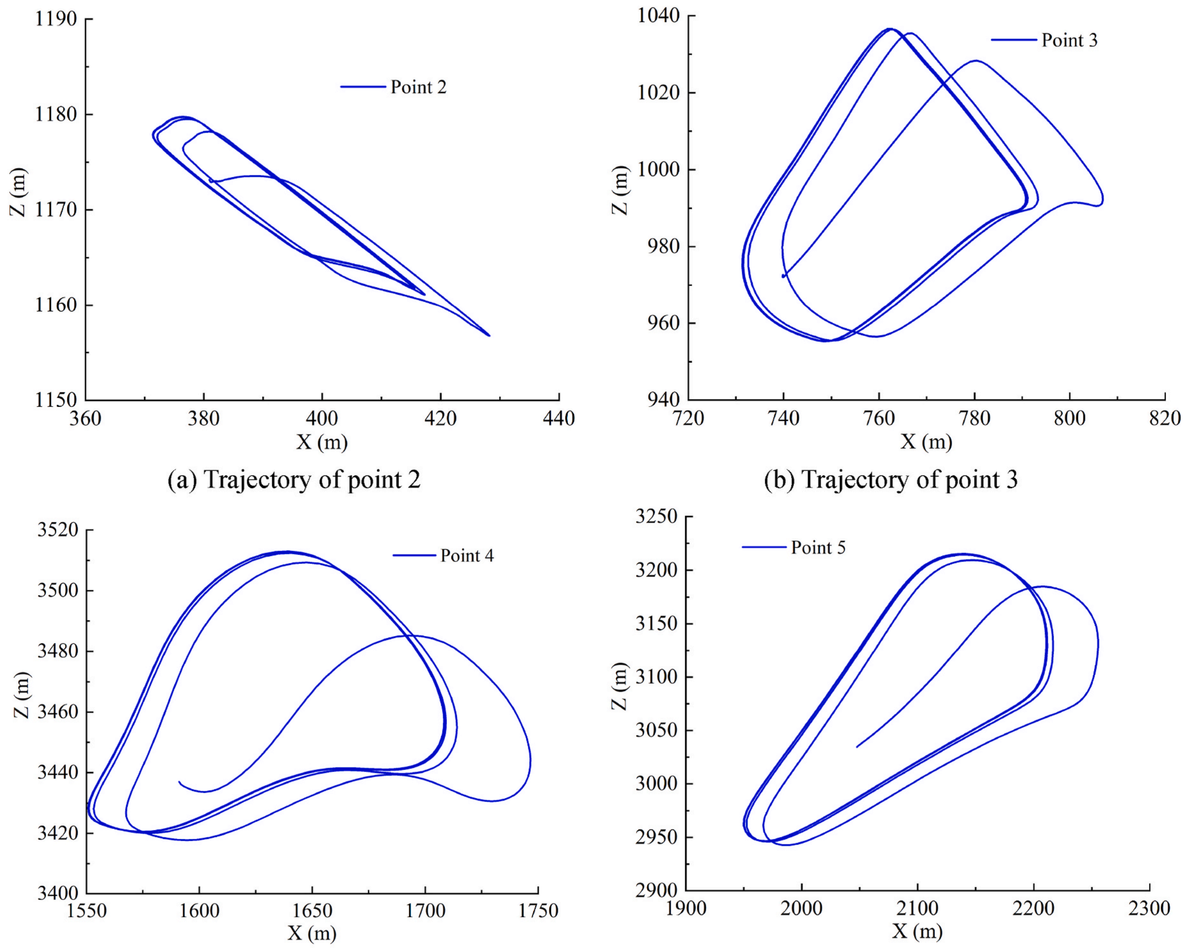

(a) Trajectory of point 2

(b) Trajectory of point 3

(c) Trajectory of point 4

(d) Trajectory of point 5

Fig. 10. Trajectories of key points.

the quadratic power of the excitation frequency. It means the cable is subjected to excitation with double frequency of vessel motion. In addition, it can be seen from Fig. 11)a that the tension and vessel displacement are not in the same phase. Due to the presence of fluid damping and tension of double frequency term, the tension amplitude increases significantly. In the case of maximum vessel displacement, the cable tension rises from 58 kN to 72 kN, and the tension increase should be paid special attention under the actual service condition.

3.2.2. Cable response under regular wave period

The periodic oscillation of the top end vessels and the cable may also be caused by wave forces. In order to investigate the response characteristics of the cable under wave frequency excitation, the cable response under the horizontal motion of the vessel with a frequency of

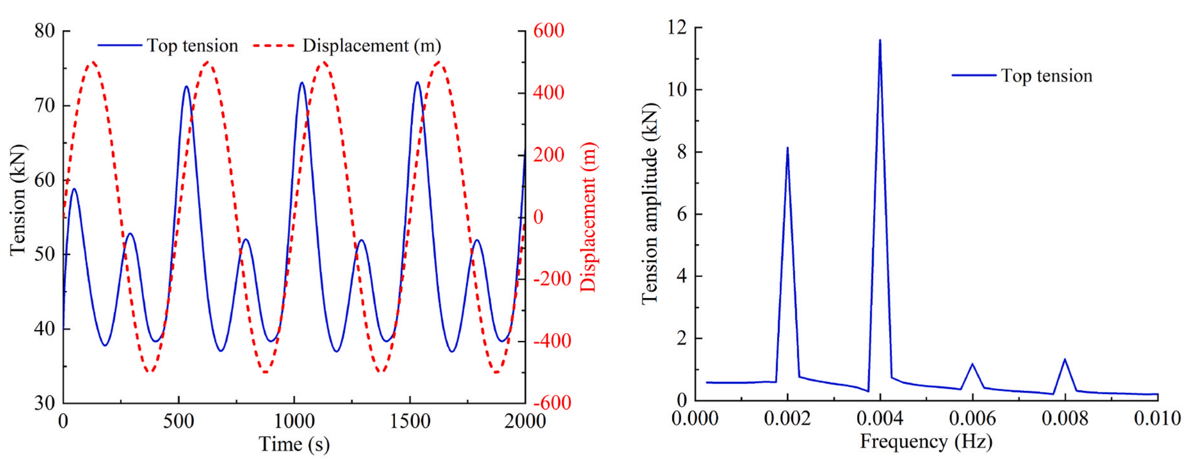

(a) Time history of top tension

(b) Frequency spectrum of top tension

Fig. 11. Time history and frequency spectrum of top tension.

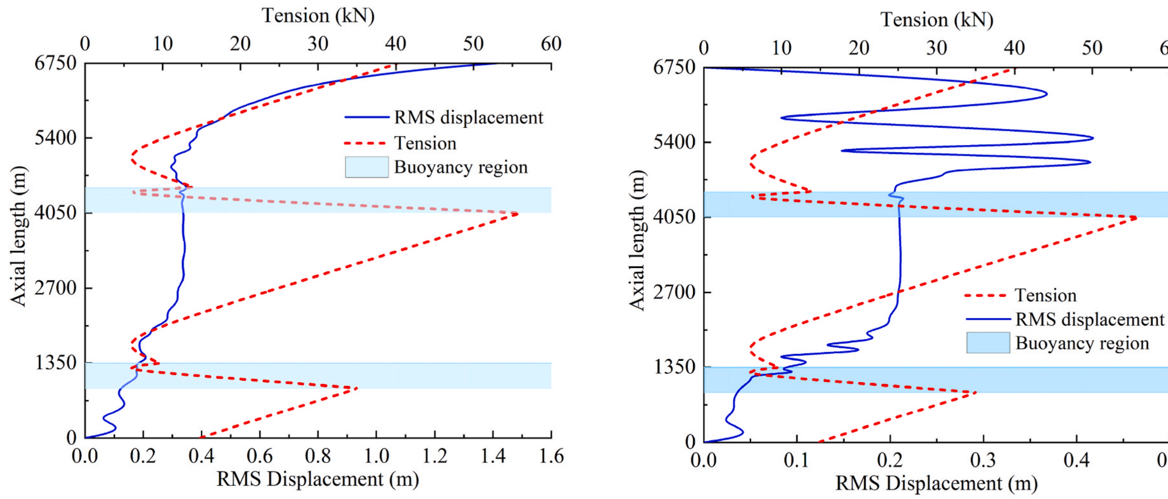

(a) RMS displacement in X direction   (b) RMS displacement in Z direction

Fig. 12. Distribution of RMS displacement and tension.

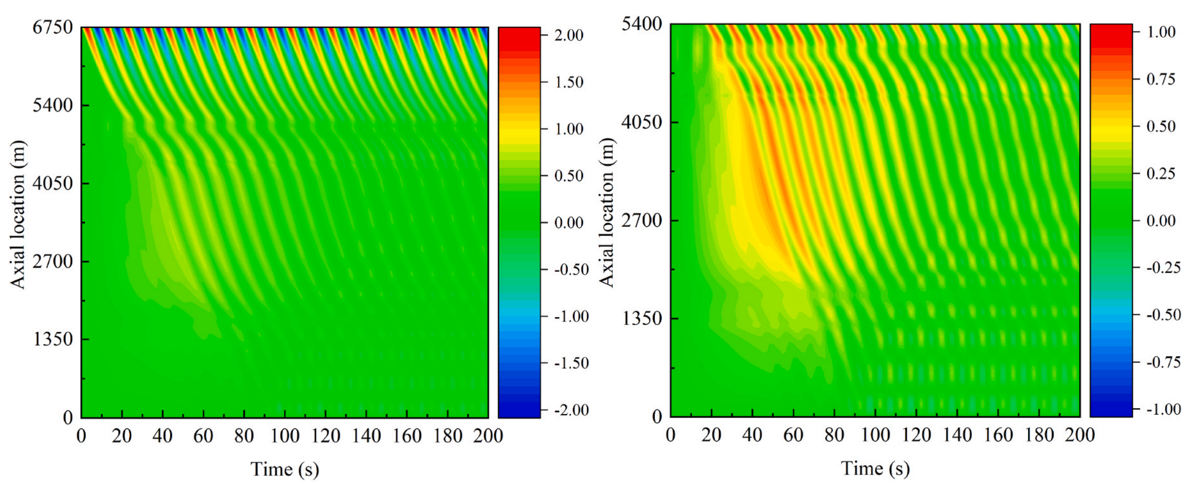

(a) Horizontal displacement   (b) Locally horizontal displacement

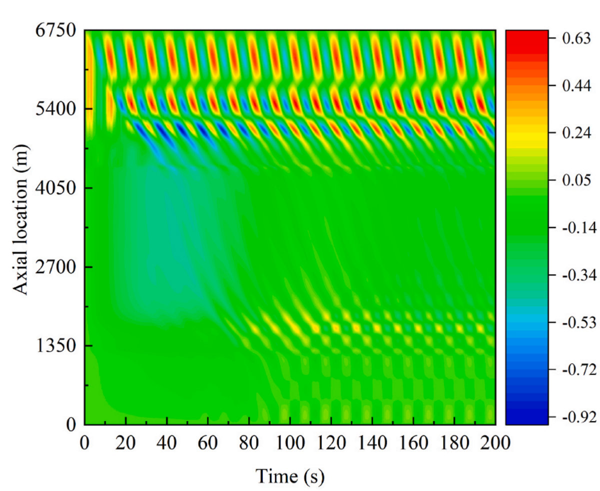

(c) Vertical displacement

Fig. 13. Spatial-temporal evolutions of cable displacements.

0.1 Hz and amplitude of 2 m is further analyzed. Fig. 12 shows the distribution of the cable's RMS (root mean square) displacement and tension along its length, and the cable length is measured from the bottom end. As shown in Fig. 12(a), the horizontal displacement response decreases in the propagation process from the top to the bottom end, and there is an apparent periodic propagation feature in the low tension region (4400–5400 m). Unlike the horizontal response, the vertical response will appear as local amplification when it propagates to the low-tension region as shown in Fig. 12(b). The maximum vertical displacement is 0.4 m, which is about 12 times the diameter. The results show that the tension near the buoyancy position will get smaller due to the buoyancy installation. And the local minimum of tension will appear at P2 and P4, which consequently makes the local maximum response occur at these points. In addition, it can be seen that the wavelength in the region with high tension is more significant (1900–2700 m), and decreases obviously in the area with low tension (1200–1900 m). And the mechanism of the temporal-spatial evolution of the dynamic responses will be discussed in detail in the next section.

Fig. 13 shows the spatial-temporal evolution of cable displacement, owing to the distributed buoyancy modules, along with axially varying and discontinuous structural properties, the response spatial-temporal evolutions become more variant. Mixed effects are coming from both standing waves and traveling waves. The horizontal displacements, shown in Fig. 13(a) and (b), are dominated by traveling waves. And the transient response lasts for about 120s, then the response enters into its steady-state stage. The propagation behaviors from top to bottom can still be seen in the cable length range of 1900–5400 m. The local maximum of vertical displacement will appear in the propagation process, as the response propagates from the top to the 4900 m position, the response amplitude increases and the wavelength decreases gradually. The response evolution is consistent with the RMS displacement result, as shown in Fig. 12. Also, due to the low tension near the position of 1600 m, the response appears to be a local maximum. The vertical displacement response also has obvious wave propagation characteristics, and the wavelength varies with tension.

4. Discussions on wave behaviors of cable with axially-varying properties

From Section 3.2, it can be seen that the response wavelength and amplitude caused by boundary motion will change due to the change of cable tension during the propagation. In this section, the influence of axial tension on response wavelength and amplitude is analyzed based on the wave propagation theory with variable parameters. The transverse free vibration equation of the beam with varying axial tension is

$$EI\frac{\partial^4 w}{\partial z^4}-\frac{\partial}{\partial z}\left(F(z)\frac{\partial w}{\partial z}\right)+m\frac{\partial^4 w}{\partial t^4}=0 \tag{8}$$

where, EI is bending stiffness, w is transverse displacement, z is axial location, m is the mass per unit length, and F is the axial tension. The aspect ratio of deep-sea flexible cables is larger than 1000, its natural frequency and stiffness are dominated by the axial stiffness (axial tension). For simplicity, the bending stiffness is ignored here. Setting EI to 0, the above equation is simplified as

$$F(z)\frac{\partial^2 w}{\partial z^2}+\frac{\partial F}{\partial z}\frac{\partial w}{\partial z}=m\frac{\partial^4 w}{\partial t^4} \tag{9}$$

Assuming that the axial force changes linearly along the axial length, i.e., $F(z)=hz$, the above formula can be expanded as

$$hz\frac{\partial^2 w}{\partial z^2}+h\frac{\partial w}{\partial z}=m\frac{\partial^4 w}{\partial t^4} \tag{10}$$

where h is constant. The variable separation method is used to solve the problem, and the deflection is written as the product of space term and time term

$$w(z,t)=Z(z)T(t) \tag{11}$$

Substituting Eq. (11) into Eq. (10), we can obtain

$$\ddot{T}+\frac{\lambda h}{m}T=0 \tag{12}$$

$$zZ''+Z'+\lambda Z=0 \tag{13}$$

where λ is a non-negative constant. The solution of Eq. (12) is

$$T(t)=A\cos\omega t+B\sin\omega t \tag{14}$$

where $\omega=\sqrt{\lambda h/m}$. Introduce the parameter $s=2\sqrt{z\lambda}$, and substituting s into Eq. (13) we obtain

$$\frac{d^2Z}{ds^2}+\frac{1}{s}\frac{dZ}{ds}+Z=0 \tag{15}$$

The above equation is the zero-order Bessel equation, and the solution of the equation is

$$Z(s)=CJ_0(s)+DY_0(s)=CJ_0\left(2\sqrt{\lambda z}\right)+DY_0\left(2\sqrt{\lambda z}\right) \tag{16}$$

where J_0 is the first type of Bessel function, and Y_0 is the second type of Bessel function. The solution of Eq. (10) is

$$w(z,t)=\left[CJ_0\left(2\sqrt{\lambda z}\right)+DY_0\left(2\sqrt{\lambda z}\right)\right](A\cos\omega t+B\sin\omega t) \tag{17}$$

Considering simply supported boundary conditions at both ends

$$\begin{array}{ll} w(0,t)=0 & z=0 \\ w(L,t)=0 & z=L \end{array} \tag{18}$$

where L is the structure length. Substituting Eq. (17) into Eq. (18) we can get

$$A=D=0 \quad J_0\left(2\sqrt{\lambda L}\right)=0 \tag{19}$$

The solution of the equation can be obtained

$$w(z,t)=C_0J_0\left(2\sqrt{\lambda z}\right)\sin\omega t \tag{20}$$

where C_0 is constant. Without loss of generality, we set C0 as 1, Fig. 14 shows the variation of response amplitude, wavelength and tension along the length. It can be seen that with the increase of tension, the response amplitude gradually decreases and the wavelength gradually increases. Therefore, the mechanism of axially varying tension on the wavelength and amplitude of cable response can be explained

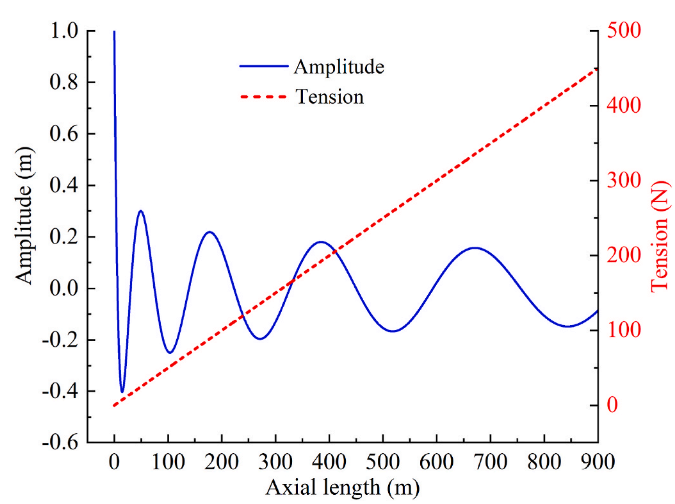

Fig. 14. Impacts of axially-varying properties on response wavelength and amplitude.

theoretically based on the wave propagation theory with variable parameters.

5. Conclusions

In this study, the dynamic response analysis model of ultra-deepwater cable is developed, based on the finite element approach combining with the coupling hydrodynamic model. The cable tension, displacement and configuration variations caused by the movements of the top vessel and the bottom mining vehicle are calculated, and the cable response and wave propagation characteristics are examined. Finally, the impacts of non-uniform structural properties on cable response and wave propagation behaviors are analyzed using the wave propagation theory of structure with axially varying properties based on the Bessel function. Our results show that: 1) The presented cable with a double-stepped configuration has a suitable compliance property, and it can reasonably bear and effectively alleviate the excitations caused by moving boundaries, such as oscillating top vessel and bottom mining vehicle operation. Compared with other configurations, such as catenary or stepped cable, the proposed double-stepped configuration would be more likely recommended in ultra-deep waters. 2) The maximum cable tensions, 24kN/72 kN under mining vehicle/vessel motions respectively, are smaller than the limited value. 3) Owing to the distributed buoyancy modules, along with axially-varying and discontinuous structural properties, the response spatial-temporal evolutions becomes more complicated. And, there exists significant mixed effect coming from both standing waves and traveling waves. 4) The axially non-uniform characteristics lead to non-monotonic changes in response amplitude and wavelength, with local peaks occurring in the low-tension region, which should be paid careful attention in structural design and safety analysis.

Declaration of competing interest

The authors declare there is no conflicts of interest regarding the publication of this paper.

Acknowledgements

The authors of this paper would like to thank the financial supports provided by the Strategic Priority Research Programme of the Chinese Academy of Sciences (Grant No. XDA22000000).

References

Adamiec-Wojcik, I., Brzozowska, L., Drag, L., 2015. An analysis of dynamics of risers during vessel motion by means of the rigid finite element method[J]. Ocean. Eng. 106, 102–114.
Cabrera, J.M., Paik, J.K., 2019. Two-phase flow induced vibrations in a marine riser conveying a fluid with rectangular pulse train mass[J]. Ocean. Eng. 174, 71–83.
Chen, W., Fu, Y., Guo, Si, et al., 2017. Review on fluid-solid coupling and dynamic response of vortex-induced vibration of slender ocean cylinders[J]. Advances in Mechanics 47 (1), 25–91 (in Chinese).
Chen, W., Guo, S., Li, Y., et al., 2021. Structural configurations and dynamic performances of flexible riser with distributed buoyancy modules based on FEM simulations[J]. Int. J. Nav. Archit. Ocean Eng. 13, 650–658.
Cheng, Y., Tang, L., Fan, T., 2020. Dynamic analysis of deepwater steel lazy wave riser with internal flow and seabed interaction using a nonlinear finite element method [J]. Ocean. Eng. 209 (4), 107498.
Fu, Y., Cao, B., Xia, J., 2019. Influence of parameter configuration of hose buoyancy for deep-sea mining system on the stress state of mining vehicle[J]. Min. Metall. Eng. 39 (2), 15–23 (in Chinese).
Gosselin, F., De Langre, E., Machado-Almeida, B.A., 2010. Drag reduction of flexible plates by reconfiguration[J]. J. Fluid Mech. 650, 319–341.
Guo, S., Chen, W., Yan, D., et al., 2022. Dynamic response and spatial-ternporal evolutions of deep-water complex configuration cables with distributed buoyancy modules[J]. Chin. J. Theor. Appl. Mech. 54 (8), 2210–2233 (in chinese).
Hsu, W.T., Thiagarajan, K.P., Manuel, L., 2017. Extreme mooring tensions due to snap loads on a floating offshore wind turbine system[J]. Mar. Struct. 55, 182–199.
Jacobsen, N., Bakker, W., Uijttewaal, W., et al., 2019. Experimental investigation of the wave-induced motion of and force distribution along a flexible stem. Journal of Fluid Mechanics [J] 880, 1036–1069.
José, Azcona, Xabier, et al., 2017. Experimental validation of a dynamic mooring lines code with tension and motion measurements of a submerged chain[J]. Ocean. Eng. 129, 415–427.
Kim, H.T., O'Reilly, O.M., 2019. Instability of catenary-type flexible risers conveying fluid in subsea environments[J]. Ocean. Eng. 173, 98–115.
Leclercq, T., De Langre, E., 2018. Reconfiguration of elastic blades in oscillatory flow[J]. J. Fluid Mech. 838, 606–630.
Leclercq, T., Peake, N., De Langre, E., 2018. Does flutter prevent drag reduction by reconfiguration? [J] Proceedings of the Royal Society A: Math. Phys. Eng. Sci. 474, 20170678.
Lee, H., Roh, M.I., Ham, S.H., et al., 2015. Dynamic simulation of the wireline riser tensioner system for a mobile offshore drilling unit based on multibody system dynamics[J]. Ocean. Eng. 106, 485–495.
Leonardo, G.R., Beatriz, M.M., Jonas, A.J., et al., 2022. Methodology for simulation of the post-failure behavior of flexible catenary risers[J]. Mar. Struct. 82, 103142.
Li, Y., Guo, S., Chen, W., et al., 2020. Analysis on restoring stiffness and its hysteresis behavior of slender catenary mooring-line[J]. Ocean. Eng. (209), 107521
Lou, M., Li, R., Wu, W., et al., 2019. Static performance analysis of deepwater compliant vertical access risers[J]. Int. J. Nav. Archit. Ocean Eng. 11, 970–979.
Mansour, A., Mekki, O.B., Montassar, S., et al., 2018. Catenary-induced geometric nonlinearity effects on cable linear vibrations[J]. J. Sound Vib. 413, 332–353.
Moore, B., Easton, A., Cabrera, J., et al., 2017. Stones development: turritella FPSO - design and fabrication of the world's deepest producing unit[C]. In: Offshore Technology Conference (OTC). Houston, Texas, USA, OTC-27663-MS.
Oh, J., Jung, D., Kim, H., et al., 2020. A study on the simulation-based installation shape design method of steel lazy wave riser (SLWR) in ultra deepwater depth[J]. Ocean. Eng. 197, 106902.
Ruan, W., Yong, B., Peng, C., 2014. Static analysis of deepwater lazy-wave umbilical on elastic seabed[J]. Ocean. Eng. 91, 73–83.
Santillan, S.T., Virgin, L.N., Plaut, R.H., 2010. Static and dynamic behavior of highly deformed risers and pipelines[J]. J. Offshore Mech. Arctic Eng. 132 (2), 021401.
Song, J.X., Chen, W.M., Yan, D.B., et al., 2021. Study on Drag Reduction of Flexible Structure under flows[C]. Xiamen, China, pp. 21–23.
Tang, D., Li, Z., Zhou, Z., et al., 2015. Effects of manganese nodules pump operation on lifting pipe vibration[J]. J. Vib. Shock 34 (23), 149–152, 160.
Tian Y, Hou Y, Pires F, et al. Tensioned step riser configuration for ultra-deep application [C], International Conference on Ocean, Offshore and Arctic Engineering. OMAE2015. V05AT04A056.
Vásquez, J.A.M., Avila, J., 2021. Three-dimensional dynamic behaviour of flexible catenary risers with an internal slug flow[J]. J. Fluid Struct. 107, 103409.
Vogel, S., 2015. Drag and flexibility in sessile Organisms1[J]. Integr. Comp. Biol. 24, 37–44.
Wang, J., Duan, M., 2015. A nonlinear model for deepwater steel lazy-wave riser configuration with ocean current and internal flow[J]. Ocean. Eng. 94 (15), 155–162.
Yin, D., Passano, E., Lie, H., et al., 2018. Experimental and numerical study of a top tensioned riser subjected to vessel motion[J]. Ocean. Eng. 171, 565–574.
Yu, Y., Wu, F., Yu, J., et al., 2022. Response analysis of compound configuration of LwSCR[J]. J. Tianjin Univ. 55 (1), 11 (in Chinese).